NANO LETTERS

XXXX
Vol. xx, No. x
-

Effect of Twinning on the Photoluminescence and Photoelectrochemical Properties of Indium Phosphide Nanowires Grown on Silicon (111)

Robyn L. Woo,[†] Rui Xiao,[‡] Yoji Kobayashi,[‡] Li Gao,[†] Niti Goel,[§] Mantu K. Hudait,[||] Thomas E. Mallouk,*[,‡] and R. F. Hicks*[,†]

Department of Chemical and Biomolecular Engineering, University of California, Los Angeles, California 90095, Department of Chemistry, Pennsylvania State University, University Park, Pennsylvania 16802, Intel Corporation, Santa Clara, California 95052, and Intel Corporation, Hillsboro, Oregon 97124

Received August 10, 2008; Revised Manuscript Received September 23, 2008

ABSTRACT

The relationship between crystal quality and the properties of indium phosphide nanowires grown on silicon (111) has been studied by transmission electron microscopy, photoluminescence spectroscopy, and photoelectrochemistry. Wires with no defects and with {111} twin boundaries parallel and perpendicular to the growth direction were obtained by metalorganic vapor-phase epitaxy using liquid indium catalyst. Room temperature photoluminescence from the defect-free nanowires is ~7 times more intense than that from the wires with twin boundaries. An open-circuit photovoltage of 100 mV is observed for photoelectrochemical cells made with the defect-free nanowires, whereas no photovoltage is recorded for those with twins.

Introduction. The integration of compound semiconductor devices on silicon substrates has been examined for many years.[1−3] Successful integration of III−V devices onto silicon-integrated circuits would allow for new architectures with much greater functionality.[4−8] Of particular interest to us is the integration of indium phosphide on silicon, since indium phosphide is a technologically important material and widely used in high-speed electronics.[9−11] In addition, indium phosphide is an interesting photoelectrode material because of the high reported photovoltage of liquid junction cells fabricated with p-type InP.[12,13] However, the principal difficulties with the integration of InP on Si are the presence of a polar/nonpolar interface and the large lattice mismatch between the two semiconductors. These properties result in high defect densities in the III−V materials that degrade device performance.[8,14,15] One way to tackle this problem is to fabricate InP devices out of one-dimensional, free-standing nanowires, which are very good at accommodating lattice strain and thermal mismatch.[16,17]

Most indium phosphide nanowires (NW) are prepared by vapor−liquid−solid (VLS) growth using gold catalysts.[18] The possibility of gold contamination of the silicon integrated circuits is problematic since Au introduces impurity states that adversely affect transistor and solar cell performance.[19] Self-catalyzed growth using liquid indium droplets may overcome this problem. In addition, InP nanowires are known to possess twinning defects due to the low stacking fault energy of the semiconductor crystal.[20,21] These defects may potentially be a problem, yet, there is no report on how they affect the solid-state physics of the InP nanowires.

In this report, we investigate the relationship between the crystal quality and optoelectronic properties of InP nanowires fabricated with liquid indium catalyst. Characterization by transmission electron microscopy (TEM), photoluminescence spectroscopy (PL), and photoelectrochemistry indicate that twins in the InP wires act as carrier recombination centers, substantially quenching the photoluminescence and eliminating the open circuit photovoltage in the electrochemical cell.

Experimental Methods. The growth experiments were carried out in a Veeco D125 metalorganic vapor-phase epitaxy (MOVPE) reactor using trimethylindium (TMIn) and *tert*-butylphosphine (TBP). Two different types of substrates,

* Corresponding authors, rhicks@ucla.edu and tom@chem.psu.edu.
[†] University of California, Los Angeles.
[‡] Pennsylvania State University.
[§] Intel Corp., Santa Clara.
[||] Intel Corp., Hillsboro.

10.1021/nl802433u CCC: $40.75
Published on Web 11/04/2008

Table 1. Summary of the Growth Conditions, Substrate Orientation, and Defects Observed for Samples A, B, and C

sample	recipe	substrate	annealing	defects	type	statistics
A	1	Si(111) 4° miscut	yes	no		8 out of 8
B	2	Si(111) 4° miscut	no	yes	{111} twins $\parallel z$-axis	5 out of 8
C	2	Si(111) 0° miscut	no	yes	{111} twins $\perp z$-axis	13 out of 15

Si(111) with 0° and 4° miscut angles, were used. They both were boron doped with resistivity of 0.002−0.008 and 1932−2110 Ω·cm, respectively. The Si wafers were cleaned in 5% hydrofluoric acid solution for 30 s and loaded immediately into the MOVPE reactor. Two different growth recipes were used. In recipe 1, the wafers were annealed at 600 °C in 1.0 mmol/min of flowing TBP for 5 min. Then the temperature was lowered to 350 °C, and indium droplets were deposited by feeding 20 μmol/min of TMIn for 0.5 min. Next, the InP nanowires were deposited by feeding TBP and TMIn at a P/In mole ratio of 54. Following 15 min of growth, the samples were cooled down in flowing H_2 for 10 min to 30 °C. In recipe 2, the growth steps were exactly the same as in the first recipe, except that the substrate annealing step was omitted and a P/In mole ratio of 75 was used. A constant TBP mole fraction of 7.2×10^{-4} was used in a hydrogen gas flow at 60 Torr total pressure. After deposition, the InP nanowires were examined using a Hitachi S4700 field emission scanning electron microscope (SEM).

The epitaxial materials were further characterized by transmission electron microscopy (TEM), photoluminescence spectroscopy (PL), and liquid-junction photoelectrochemistry. For TEM, the samples were prepared by stripping the nanowires from the substrate, dispersing them in ethanol by brief sonication, and then depositing the concentrated ethanol suspension onto a TEM grid. Images were recorded with either a JEOL 2010F or a JEOL 2010 LaB_6 transmission electron microscope operating at 200 kV. Photoluminescence measurements were performed directly on the nanowire arrays on Si(111) using a Phillips PLM 100 spectrometer. The photoexcitation source was the 488 nm line of an argon ion laser.

Photoelectrochemical measurements were carried out in a three-electrode cell, which included an Ag/Ag(NO_3) (in CH_3CN) reference electrode, a Pt counter electrode, and a working electrode made from the InP nanowire array on the Si substrate. The back metallic contact was insulated with a combination of glass tubing and epoxy, leaving only the nanowire-bearing face of the InP NW electrode exposed. The InP NW arrays were briefly etched in 1% Br_2/methanol solution and then rinsed with methanol. The InP NW photoelectrode was immersed in a 40 mL glass vial containing a solution of 1 mM methyl viologen hexafluorophosphate ($MV(PF_6)_2$) and 100 mM tetrabutylammonium perchlorate (n-Bu_4NClO_4) in dry CH_3CN. Argon was bubbled into the cell to deoxygenate the solution. Cyclic voltammetry was performed using a BAS 100B instrument from Princeton Analytical Systems. The scan rate was 50 mV/s, and the scan was initiated from the most anodic (positive) potential. An Hg/Xe arc lamp with an AM 1.5 filter was used as the light source with an illumination power density of 0.84 W/cm^2 at the electrode surface.

Results. Table 1 summarizes the growth conditions and substrates used for the three types of nanowire arrays, designated A, B, and C. For sample A, InP nanowires were grown on Si(111) with 4° miscut using growth recipe 1, whereas for sample B, the wires were grown on the same substrate using growth recipe 2. For sample C, InP nanowires were grown on Si(111) with no miscut using growth recipe 2. The z-axis is designated as the growth direction. Structural information acquired by TEM is also summarized in the table.

Figure 1 shows scanning electron micrographs of samples A, B, and C. For sample A, the average density is 1.4×10^9 cm^{-2}, the diameter is 50−90 nm, and the length is ∼2 μm. For sample B, the average density is 1.2×10^9 cm^{-2}, the diameter is 50−60 nm, and the length is ∼1.5 μm. For sample C, the average density is 2.1×10^9 cm^{-2}, the diameter is about 30 nm, and the length is ∼2.3 μm.

Figure 2a shows a transmission electron micrograph of an InP nanowire from sample A. The inset is a selective area electron diffraction (SAED) pattern of the same wire. Indexing the diffraction pattern reveals that the wire has a growth direction of $[\bar{1}\bar{1}1]$. Figure 2b shows a higher-resolution TEM image of the edge of the nanowire from the region within the circle. The picture reveals the (111) lattice fringes with a spacing of 3.34 Å. Both the SAED pattern

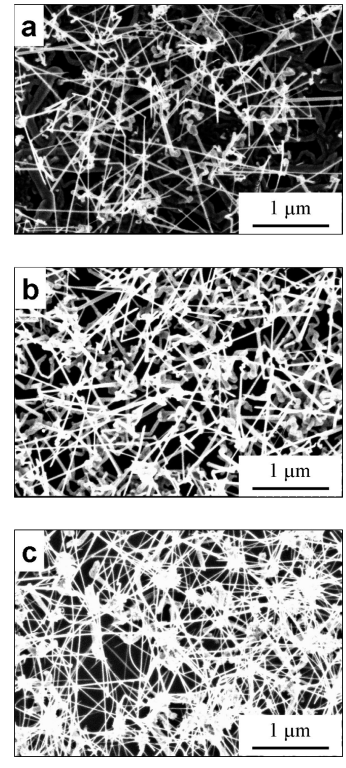

Figure 1. Scanning electron micrographs of (a) sample A, (b) sample B, and (c) sample C.

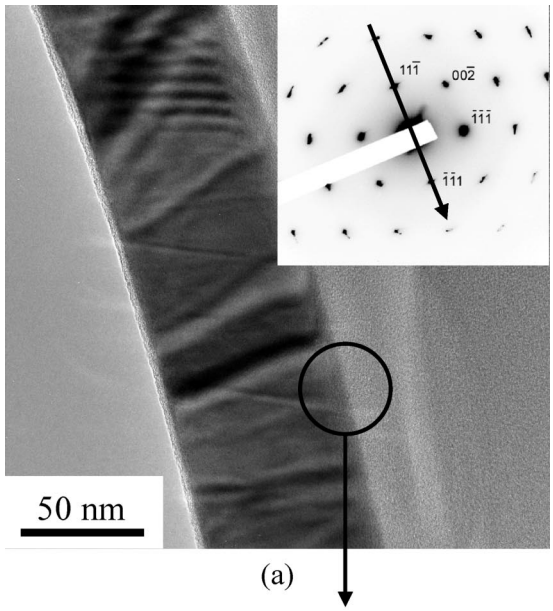

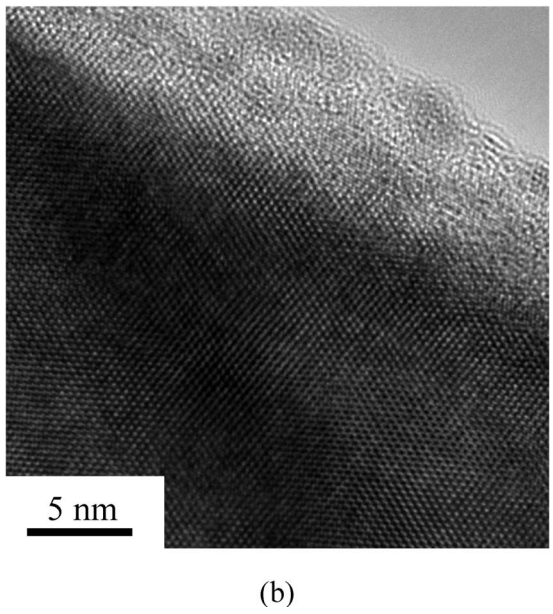

Figure 2. (a) TEM image of an InP nanowire from sample A. The inset shows a selective area electron diffraction pattern taken from the [$\bar{1}$10] zone axis. (b) High-resolution TEM image of the same wire.

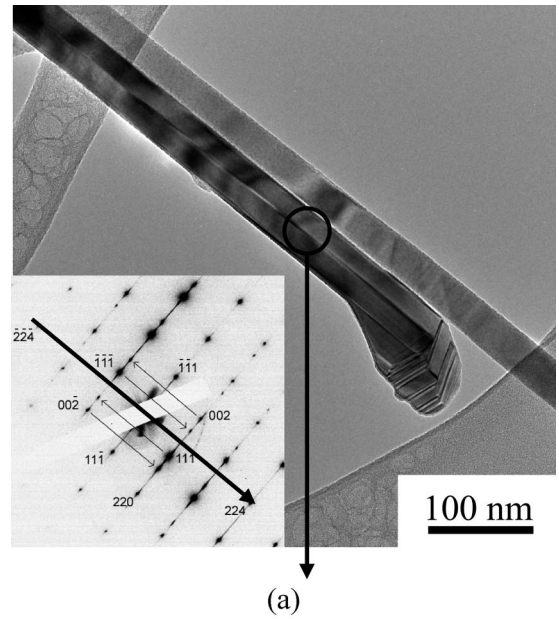

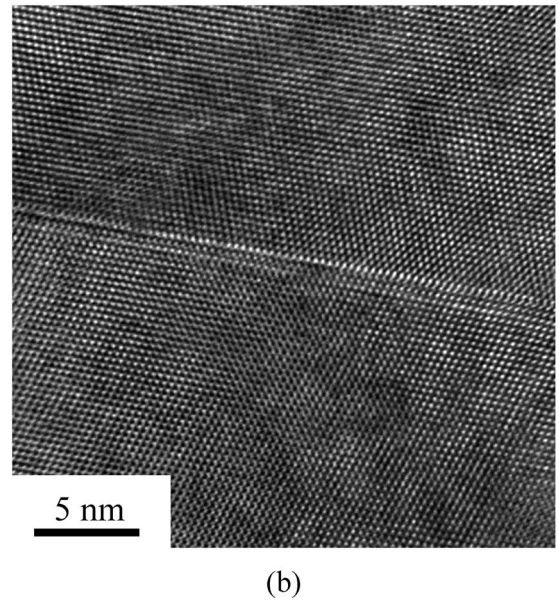

Figure 3. (a) TEM image of an InP nanowire from sample B. The inset shows a selective area electron diffraction pattern taken from the [$\bar{1}$10] zone axis. (b) High-resolution TEM image of the same wire.

and lattice fringes seen by high-resolution transmission electron microscopy (HR-TEM) indicate that the wire is defect-free and has the zinc blende crystal structure. From sample A, a total of eight wires were analyzed by TEM and all of them were defect-free. Note that the amorphous oxide skin surrounding the nanowires is revealed in the micrographs. The estimated thickness of this layer is 5.0 nm.

Figure 3a presents an electron micrograph of an InP nanowire from sample B. A planar defect along the *z*-axis of the wire is seen in the image. In addition, the cross hatches of other {111} twin boundaries are visible at the end of the wire. This end is the starting point of InP nanowire growth on the Si substrate, since the tip of the VLS-grown wire is attached to the metal droplet.[18] The inset shows an SAED pattern taken from the body of the same wire. Indexing the diffraction pattern reveals that the wire has a growth direction of [224] and a defect plane parallel to the growth direction. A HR-TEM image of the area highlighted in the circle is shown in Figure 3b. Here, we can see the planar defect, specifically, a ($\bar{1}\bar{1}$1) twin plane parallel to the wire axis. A spacing of 3.58Å is measured from (111) lattice fringes on the image. Five out of eight wires analyzed by TEM show planar defects parallel to the growth direction.

Figure 4a shows an electron micrograph of an InP nanowire from sample C. Closely spaced arrays of planar defects perpendicular to the wire axis are visible in the image. This is confirmed by the severe streaking along the growth direction seen in the SAED pattern. The diffraction pattern reveals that the wire has a growth direction of [111]. The HR-TEM image in Figure 4b shows a high density of (111)

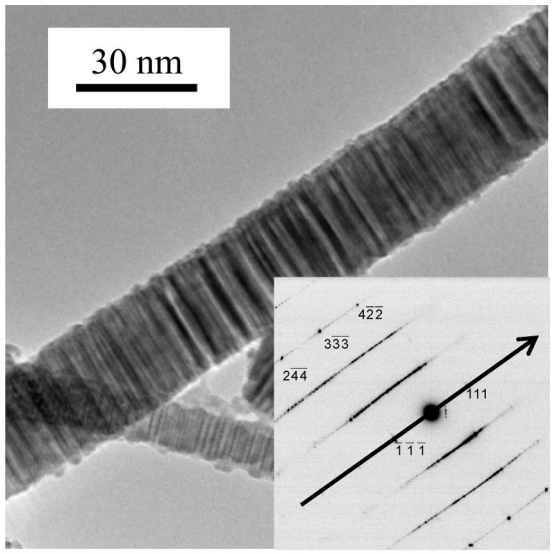

(a)

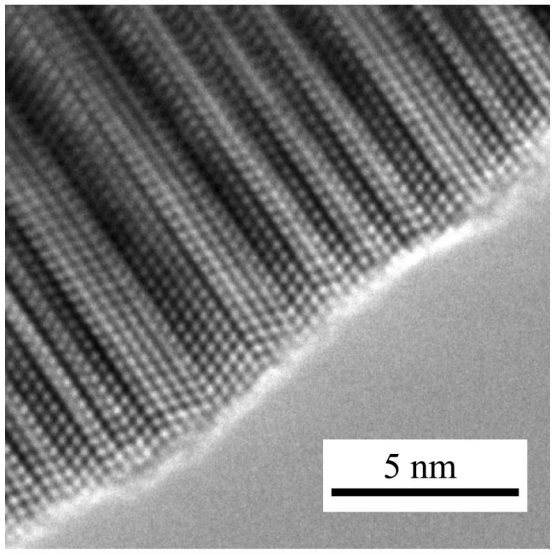

(b)

Figure 4. (a) TEM image of an InP nanowire from sample C. The inset shows a selective area electron diffraction pattern taken from the [0$\bar{1}$1] zone axis. (b) High-resolution TEM image of the same wire.

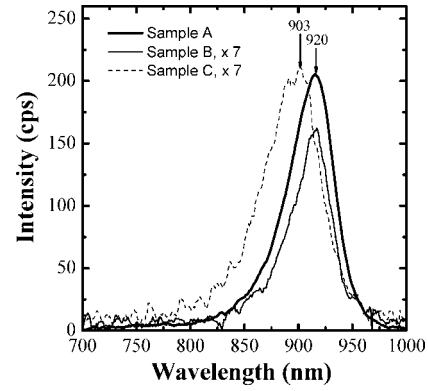

Figure 5. Normalized room-temperature photoluminescence spectra of InP nanowires from samples A, B, and C.

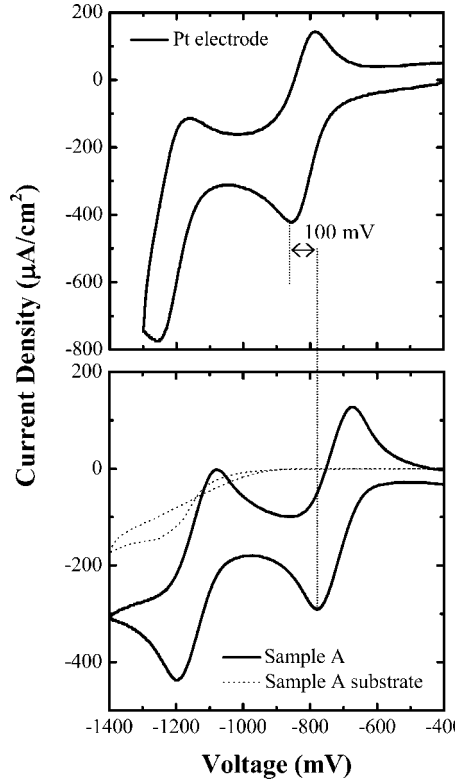

Figure 6. Cyclic voltammograms (50 mV/s) of the Pt disk electrode, the InP nanowire electrode made from sample A under illumination, and the silicon substrate for sample A under illumination.

twin boundaries perpendicular to the wire axis. Between twin boundaries are domains of different lengths that have the zinc blende crystal structure. A spacing of 3.35 Å is measured from the (111) lattice fringes in the image. Thirteen out of fifteen wires analyzed by TEM show (111) twin boundaries normal to the wire growth direction. In the image shown in Figure 4, the oxide skin is <1.0 nm, which is significantly thinner than that seen in Figure 2.

Room-temperature photoluminescence spectra measured of samples A, B, and C are shown in Figure 5. The intensity of each spectrum has been normalized according to the estimated amount of nanowire material, A:B:C = 3.2:1.4:1.0. Samples A and B have a PL emission peak centered at 920 nm and full width at half-maximum (fwhm) of 50 and 45 nm, respectively. By contrast, sample C exhibits a peak at 903 nm and an fwhm of 63 nm. The luminescence emission at 920 nm is characteristic of bulk indium phosphide and can be attributed to emission from bound excitons.[22,23] One can see that the emission intensity from the defect-free nanowires (sample A) is approximately 7 times greater than that from the nanowires with twins (samples B and C).

Figure 6 compares the cyclic voltammetry of the illuminated InP/Si nanowire photoelectrodes fabricated from samples A with that of a dark Pt electrode. The current−voltage curves show the two cathodic and anodic peaks, corresponding to the two reductions and oxidations of the methylviologen (MV^{2+}) redox couple in the solution. At the low concentration of methylviologen used in these experiments, the current density is always low, and the difference in cathodic peak positions between the Pt and the illuminated InP electrodes can be taken as an approximate measure of

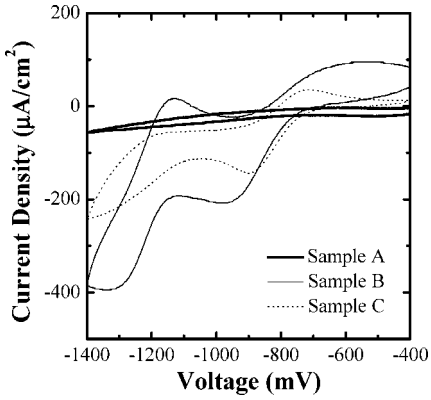

Figure 7. Cyclic voltammograms (50 mV/s) of the InP nanowire array electrodes made from samples A, B, and C in the dark.

the open circuit photovoltage of the photoelectrochemical cell. In this case, sample A shows the first cathodic peak that is approximately 100 mV positive compared to the Pt electrode. Under the same conditions, samples B and C exhibit negligible open circuit photovoltage.

In order to confirm that the photoactivity comes only from InP nanowire arrays, control experiments for the Si substrates were performed. The lower plot of Figure 6 shows that the Si substrate has very low photocurrent compared with the nanowire arrays of sample A. All the silicon wafers had no dark current without illumination. These results demonstrate that the photoelectrochemical current, as well as the dark current, comes from the InP nanowires and that the Si substrates are effectively insulated from the solution. Any differences among the photovoltages of sample A, B, and C can therefore be attributed to structural variations in the InP nanowires.

Figure 7 compares cyclic voltammograms of the InP/Si nanowire photoelectrodes fabricated from samples A, B, and C without illumination. In general, samples with measurable photocurrent will have low dark current. The InP/Si nanowire electrode fabricated from sample A exhibits negligible cathodic current in the dark. In contrast, the InP/Si nanowires fabricated from samples B and C show dark current in the same potential range. Between samples B and C, sample B exhibits higher dark current.

Discussion. Indium phosphide nanowires with and without defects were grown using different recipes and substrate orientations. Our results suggest that there might be some registry between the nanowires and the substrate used for growth. Samples B and C were prepared following the same procedure, but with 4° and 0° miscut angles relative to the normal vector from the Si(111) plane. Samples with the higher miscut angle had small (111) terraces and a high density of steps exposing {110} and {112} facets. Since the steps are favorable sites for nucleation and growth of nanowires, one should observe wires with {110} and {112} growth planes. This is confirmed by TEM, where all eight wires examined from sample B possess either λ or ξ growth directions. Conversely, most nanowires will nucleate and grow on the (111) terraces of substrate C with the 0° miscut angle. This is indeed the case as 13 out of 15 wires imaged by TEM grew along the [111] crystal axis.

Due to the low stacking fault energy of InP, this crystal easily forms twins.[20,21] For InP nanowires grown on (111) substrates, twinning has been reported several times before[24−26] and again is seen in this study (i.e., Figure 4). Insertion of a twin plane into the zinc blende crystal changes the stacking order, creating a small segment of wurtzite between two zinc blende domains. Consequently, the wire consists of a mixture of zinc blende and wurtzite along the crystal growth direction as seen in Figure 4. On the other hand, nanowires grown on the 4°-off-axis substrate exhibit twins in $(11\bar{1})$ planes. In this sample, the InP nanowires may nucleate from a combination of exposed planes and steps and upon coalescence form boundaries and twin planes such as that seen in Figure 3.

Samples A and B were prepared from the same 4°-off-axis Si(111) wafer. The InP nanowire growth procedure was the same, except that the former sample was subjected to annealing in TBP at 600 °C prior to indium droplet deposition. This annealing step is expected to passivate the Si surface with phosphorus atoms.[1] The layer of P atoms may have delayed the formation of indium droplets. Upon feeding TMIn to the reactor, a layer of indium may have wetted the surface initially, followed by In droplet nucleation at a later stage. This was verified by imaging the surface with the scanning electron microscope after 30 s of flowing TMIn through the reactor. No indium droplets were detected on the annealed substrate, whereas they were observed on the substrate that was not annealed. Continued feeding of TMIn and TBP, however, allows the indium droplets to form on top of the wetting layer with subsequent nanowire growth by VLS. Another effect of annealing the 4° miscut substrate in TBP may be to create double-height steps, which eliminates antiphase domains upon the coalescence of nearby crystal nuclei.[27−29]

Both samples A and B exhibit photoluminescence at 920 nm, which corresponds to the InP bandgap energy of 1.35 eV. By contrast, the photoluminescence peak for sample C is at 903 nm, or 1.38 eV. Note that the wurtzite crystal structure for InP exhibits a bandgap of 1.43 eV.[30] The observed blue shift in the emission band for sample C can be attributed to the intimate mixture of zinc blende and wurzite domains in the nanowires grown on the Si(111) (cf. Figure 4b).

The twins present in the nanowires on sample B and C are evidently responsible for the large drop in PL intensity compared to that of the defect-free nanowires on sample A. The twin boundaries are probably efficient recombination centers. Surface states in the crystalline zinc blende portions of the nanowires do not appear to play a major role, since the wires on samples A and B are about the same size, ~60 to 70 nm in diameter. On sample C, the wires are ~25 nm in diameter, but the PL intensity is the same as that recorded for sample B. These results clearly demonstrate the strong impact of defects on the optical emission from III/V semiconductor nanowires.

The cyclic voltammograms shown in Figures 6 and 7 support the conclusion that twinning defects act as recombination centers. A Pt electrode was used as the working

electrode, and the difference between the first cathodic peak at Pt and at the InP nanowire array was recorded as the photovoltage. Only sample A exhibited negligible cathodic current in the dark and an open circuit photovoltage of 100 meV under illumination. The 100 mV photovoltage observed for sample A is far from the 700 mV photovoltage obtained for p-type InP single crystals.[13] The relatively low photovoltage may be related to leakage across the depletion layer at the nanowire surface and the small diameter of the InP nanowires, which may yield junctions with high surface area. Nevertheless, this work provides the first demonstration of photoelectrochemical energy conversion in III/V nanowires.

In summary, indium phosphide nanowires have been grown on Si(111) without defects, with {111} twin boundaries parallel to the wire axis, and with {111} twin boundaries normal to the wire axis. Photoluminescence and liquid-junction photovoltage measurements indicate that the twins strongly attenuate the optoelectronic properties of the InP nanostructures.

Acknowledgment. Funding for this research was provided by Intel, UC-Micro program, and the Office of Basic Energy Sciences, Division of Chemical Sciences, Geosciences, and Biosciences, U.S. Department of Energy under Contract DE-FG02-05ER15749. The authors would like to thank Dr. Daniel Law and Kenneth Edmondson for their help in obtaining the photoluminescence data. Electron microscopy work was supported in part by the Pennsylvania State University Materials Research Institute NanoFabrication Network and the National Science Foundation Cooperative Agreement No. 0335765, National Nanotechnology Infrastructure Network, with Cornell University.

References

(1) Kawanami, H. *Sol. Energy Mater. Sol. Cells* **2001**, *66*, 479.
(2) De Boeck, J.; Borghs, G. *J. Cryst. Growth* **1993**, *127*, 85.
(3) Akiyama, M.; Kawarada, Y.; Kaminishi, K. *J. Cryst. Growth* **1984**, *68*, 21.
(4) F Geisz, J.; Friedman, D. J. *Semicond. Sci. Technol.* **2002**, *176*, 769.
(5) Mathine, D. L. *IEEE J. Sel. Top. Quantum Electron.* **1997**, *3*, 952.
(6) Ringle, S. A.; Carlin, J. A.; Andre, C. L.; Hudait, M. K.; Gonzalez, M.; Wilt, D. M.; Clark, E. B.; Jenkins, P.; Scheiman, D.; Allerman, A.; A Fizgerald, E.; Leitz, C. W. *Prog. Photovoltaics* **2002**, *10*, 417.
(7) Yonezu, H.; Furukawa, Y.; Abe, H.; Yoshikawa, Y.; Moon, S. Y.; Utsunu, A.; Yoshizumi, Y.; Wakahara, A.; Ohtani, M. *Opt. Mater.* **2005**, *27*, 799.
(8) Fang, S. F.; Adomi, K.; Iyer, S.; Morkoc, H.; Zabel, H.; Choi, C.; Otsuka, N. *J. Appl. Phys.* **1990**, *68*, R31.
(9) Bach, H.-G.; Schlaak, W.; Mekonnen, G. G.; Seeger, A.; Steingruber, R.; Schramm, C.; Jacumeit, G.; Ziegler, R.; Umbach, A.; Unterborsch, G.; Passenberg, W.; Ebert, W.; Eckardt, T. In *Optical Fiber Communication Conference*; Trends in Optics and Photonics, Vol. 37; Optical Society of America: Washington, DC, 2000.
(10) Camargo Silva, M. T.; Zucker, J. E.; Carrion, L. R.; Joyner, C. H.; Dentai, A. G. *IEEE J. Sel. Top. Quantum Electron.* **2000**, *6*, 26.
(11) Akage, Y.; Kawano, K.; Oku, S.; Iga, R.; Okamoto, H.; Miyamoto, Y.; Takeuchi, H. *Electron. Lett.* **2001**, *37*, 299.
(12) Heller, A.; Miller, B.; Lewerenz, H. J.; Bachmann, K. J. *J. Am. Chem. Soc.* **1980**, *102*, 6555.
(13) Dominey, R. N.; Lewis, N. S.; Wrighton, M. S. *J. Am. Chem. Soc.* **1981**, *103*, 1261.
(14) Drory, M. D.; Evans, A. G. *J. Am. Ceram. Soc.* **1990**, *73*, 634.
(15) Sugo, M.; Yamaguchi, M. *Appl. Phys. Lett.* **1989**, *54*, 1754.
(16) Wagner, R. S. In *Whisker Technology*; Levitt, A. P., Ed.; Wiley: New York, 1970.
(17) Wong, E. W.; Sheehan, P. E.; Lieber, C. M. *Science* **1997**, *277*, 1971.
(18) Wagner, R. S.; Ellis, W. C. *Appl. Phys. Lett.* **1964**, *4*, 89.
(19) Pantelides, S. T., *Deep Centers in Semiconductors*; Gordon and Breach: New York, 1986.
(20) *III-Vs Review, The Advanced Semiconductor Magazine* 2005 *18* 5 30
(21) Asahi, T.; Kainosho, K.; Kamiya, T.; Nozaki, T.; Matsuda, Y.; Oda, O. *Jpn. J. Appl. Phys.* **1999**, *38*, 977.
(22) Wang, J.; Gudiksen, M. S.; Duan, X.; Cui, Y.; Lieber, C. M. *Science* **2001**, *293*, 1455.
(23) White, A. M.; Dean, P. J.; Taylor, L. L.; Clarke, R. C. *J. Phys. C: Solid State Phys.* **1972**, *5*, L110.
(24) Mattila, M.; Hakkarainen, T.; Jiang, H.; Kauppinen, E. I.; Lipsanen, H. *Nanotechnology* **2007**, *18*, 155301.
(25) Bhunia, S.; Kawamura, T.; Fujikawa, S.; Nakashima, H.; Furukawa, K.; Torimitsu, K.; Watanabe, Y. *Thin Solid Films* **2004**, *464−465*, 244.
(26) Novotny, C. J.; Yu, P. K. L. *Appl. Phys. Lett.* **2005**, *87*, 203111.
(27) Kawabe, M.; Ueda, T.; Takasugi, H. *Jpn. J. Appl. Phys.* **1987**, *26*, L114.
(28) Becker, R. S.; Klitsner, T.; Vickers, J. S. *J. Microsc.* **1988**, *152*, 157.
(29) Varrio, J.; Asonen, H.; Lammasniemi, J.; Rakennus, and Pessa, K. *Appl. Phys. Lett.* **1989**, *55*, 1987.
(30) Kobayashi, Y.; Fukui, M.; Motohisa, J.; Fukui, T. *Physica E* **2008**, *40*, 2204.

NL802433U